ISSN 1674-1056
http://cpb.iphy.ac.cn
http://iopscience.iop.org/cpb
中国物理 B
Chinese Physics
中国物理
Chinese Physics B

Experimental and numerical investigation of a Hall thruster with a chamfered channel wall

Hong Li(李鸿), Guo-Jun Xia(夏国俊), Wei Mao(毛威), Jin-Wen Liu(刘金文), Yong-Jie Ding(丁永杰), Da-Ren Yu(于达仁), Xiao-Gang Wang(王晓钢)

Citation: Chin. Phys. B . 2018, 27(10): 105209. **doi:** 10.1088/1674-1056/27/10/105209

Journal homepage: http://cpb.iphy.ac.cn; http://iopscience.iop.org/cpb

What follows is a list of articles you may be interested in

Influence of channel length on discharge performance of anode layer Hall thruster studied by particle-in-cell simulation

Xi-Feng Cao(曹希峰), Hui Liu(刘辉), Wen-Jia Jiang(蒋文嘉), Zhong-Xi Ning(宁中喜), Run Li(黎润), Da-Ren Yu(于达仁)
Chin. Phys. B . 2018, 27(8): 085204. **doi:** 10.1088/1674-1056/27/8/085204

Particle-in-cell simulation for the effect of magnetic cusp on discharge characteristics in a cylindrical Hall thruster

Sheng-Tao Liang(梁圣涛), Hui Liu(刘辉), Da-Ren Yu(于达仁)
Chin. Phys. B . 2018, 27(4): 045201. **doi:** 10.1088/1674-1056/27/4/045201

Low-frequency oscillations in Hall thrusters

Wei Li-Qiu, Han Liang, Yu Da-Ren, Guo Ning
Chin. Phys. B . 2015, 24(5): 055201. **doi:** 10.1088/1674-1056/24/5/055201

Characteristics of wall sheath and secondary electron emission under different electron temperatures in a Hall thruster

Duan Ping, Qin Hai-Juan, Zhou Xin-Wei, Cao An-Ning, Chen Long, Gao Hong
Chin. Phys. B . 2014, 23(7): 075203. **doi:** 10.1088/1674-1056/23/7/075203

Numerical study on the electron-wall interaction in a Hall thruster with segmented electrodes placed at the channel exit

Qing Shao-Wei, E Peng, Duan Ping, Xu Dian-Guo
Chin. Phys. B . 2013, 22(8): 085203. **doi:** 10.1088/1674-1056/22/8/085203

Experimental and numerical investigation of a Hall thruster with a chamfered channel wall*

Hong Li(李鸿)[1,†], Guo-Jun Xia(夏国俊)[1], Wei Mao(毛威)[2], Jin-Wen Liu(刘金文)[1], Yong-Jie Ding(丁永杰)[1,‡], Da-Ren Yu(于达仁)[1], and Xiao-Gang Wang(王晓钢)[3]

[1] *Plasma Propulsion Laboratory, Harbin Institute of Technology, Harbin* 150001, *China*
[2] *Beijing Institute of Control Engineering, Beijing* 100190, *China*
[3] *Department of Physics, Harbin Institute of Technology, Harbin* 150001, *China*

(Received 18 October 2017; revised manuscript received 3 July 2018; published online 27 September 2018)

A discharge channel with a chamfered wall not only has application in the design of modern Hall thrusters, but also exists where the channel wall is eroded, and so is a common status for these units. In this paper, the laws and mechanisms that govern the effect of the chamfered wall on the performance of a Hall thruster are investigated. By applying both experimental measurement and particle-in-cell simulation, it is determined that there is a moderate chamfer angle that can further improve the optimal performance obtained with a straight channel. This is because the chamfering of the wall near the channel exit can enhance ion acceleration and effectively reduce ion recombination on the wall, which is favorable to the promotion of the thrust and efficiency. However, the chamfer angle should not be too large; otherwise, both the density of the propellant gas and the distribution of the plasma potential in the channel are influenced, which is undesirable for efficient propellant utilization and beam concentration. Therefore, it is suggested that the chamfer shape of the channel wall is an important factor that must be carefully considered in the design of Hall thrusters.

Keywords: Hall thruster, chamfered wall, discharge performance, physical mechanism

PACS: 52.75.Di, 52.30.–q, 52.65.Rr **DOI:** 10.1088/1674-1056/27/10/105209

1. Introduction

A Hall thruster is a type of advanced electric propulsion used in space vehicles for station keeping, orbit raising, and deep space exploration. Compared with chemical propulsion, the Hall thruster has the advantage of high specific impulse, which can greatly increase either the payload ratio of the satellites or the total impulse of the propulsion system. Currently, it is widely applied in the aerospace industry and is considered to be a promising propulsion technology for future development and application.[1]

In principle, the Hall thruster is a plasma discharge device in which orthogonal electric and magnetic fields are utilized to ionize and accelerate the propellant gas.[2] It has a quasi-axisymmetric structure; the propellant ionization and acceleration usually take place inside an annular channel surrounded by two lateral walls. To guarantee the efficiency of the propellant utilization, light-mass electrons are magnetically confined and trapped inside the channel to ionize gaseous neutrals through collision. Heavy-mass ions, which are not magnetized, are accelerated electrostatically out of the channel to produce thrust.

A Hall thruster with a chamfered channel wall is a frequently encountered situation. At present, Hall thrusters can be categorized as unshielded (US) and magnetically shielded (MS), depending on whether the channel wall suffers energetic ion sputtering and erosion or not. As for the classical models of Hall thrusters, such as the SPT-100[3] and PPS1350,[4] they are unshielded. In a US thruster, the channel is generally designed to be straight with a constant cross-sectional area. This configuration has the advantage of simplifying the thruster design. However, the wall section close to the channel exit always suffers a severe ion sputtering and erosion effect, which results in a chamfering of the channel wall.[5] In contrast, some modern models of Hall thrusters, such as the H6,[6] MaSMi-60,[7] and PPS-FLEX,[8] are magnetically shielded. In an MS thruster, the channel wall is artificially chamfered; furthermore, the magnetic field near the surface of the chamfered wall is specifically designed to avoid ion sputtering and erosion. An MS Hall thruster can maintain its initial chamfered wall shape well, which leads to a great extension of the thruster lifetime.[9,10]

A few studies have been reported on the effect of the chamfered channel wall, or the channel configuration from a more general perspective, on the discharge of Hall thrusters. In the scope of US thrusters, Arhipov *et al.* numerically found that the chamfering of the channel wall is favorable for the decrease of the wall loss; moreover, an increase of the chamfer angle results in an increase in both the thrust and efficiency.[11]

*Project supported by the National Natural Science Foundation of China (Grant Nos. 51507040, 51777045 and 51736003), the Fundamental Research Funds for the Central Universities, China (Grant No. HIT. NSRIF. 2015079), and the Research Program, China (Grant No. JSZL2016203C006).

†Corresponding author. E-mail: lihong@hit.edu.cn
‡Corresponding author. E-mail: dingyongjie@hit.edu.cn

© 2018 Chinese Physical Society and IOP Publishing Ltd

Yamamoto *et al.* experimentally found that the chamfering of the channel wall affects the relationship between the oscillation amplitude and the magnetic field intensity greatly.[12] Raitses *et al.* experimentally found that the propellant utilization would be effectively improved by reducing the cross-sectional area of the channel near the anode when the propellant flow rate is low.[13] In the scope of MS thrusters, Mikellides *et al.* provided strong theoretical and experimental evidence that the design of the chamfered wall shape should ensure that the magnetic field lines graze the wall corner and the grazing line must extend deep into the channel.[14,15] These two principles are sufficient to warrant the effectiveness of magnetic shielding. However, the issue that whether both the MS effect and the optimal performance are achieved together or not has not been addressed so far.

In this paper, experimental and numerical investigations are conducted on a US Hall thruster. The focus is on an evaluation of the influence of the wall chamfer angle, along with the magnetic field intensity, on the thruster discharge and performance. Although a related study on an MS Hall thruster is not presented in this paper, it is believed that the findings on the US Hall thruster are fundamental and common, which will motivate and inspire the study of the optimal design of the chamfered wall shape in MS thrusters. The rest of the paper is organized as follows. Section 2 describes the experimental design and apparatus, as well as the numerical model and simulation method. The experimental result is presented and analyzed with the support of simulation results in Section 3. Conclusions are summed up in Section 4.

2. Research methods

2.1. Experimental design and apparatus

The first step in the preparation of the experiment is to choose which section of the channel wall to be chamfered. Here, the section corresponding to the acceleration region is selected. This selection is theoretically expected to preserve the propellant utilization and reduce the ion loss on the wall, which is favorable for the performance optimization. Furthermore, as the sputtered and eroded section of the channel wall is located right in the acceleration region, this region with an artificial chamfered configuration may approximate the status of a US thruster at a specific stage of its lifetime. Consequently, the discharge characteristics of a US thruster during its entire lifetime could be estimated readily.

The inherent back-sputtering that occurs in the ground test of a US Hall thruster makes the position of the acceleration region well identified. The ground test is usually conducted in a tank which is evacuated by pumps to simulate the ultra-low pressure environment of space. The energetic ions ejected out of the thruster channel can bombard the tank surface directly and sputter out the tank material, which then flows back into the thruster channel and deposits on the wall.[16] Generally, the channel wall, which is made of ceramics based on boron nitride, is white in color; however, as the tank material is mainly iron and carbon, the deposition causes the wall to turn black. In most of the acceleration region of a US Hall thruster, the wall erosion rate is generally greater than the deposition rate; this section of the wall (namely the erosion belt) thus remains white. Contrarily, the rest section of the wall is black. This feature allows one to identify the position where the wall surface changes obviously from black to white as the starting position of the main acceleration region, namely the position where the channel wall begins to be chamfered.

A US Hall thruster prototype P100, as shown in Fig. 1, is used in the experiments. Its nominal power is 1.5 kW and its original channel configuration is straight. The P100 has the identical radial dimensions as the SPT-100. The inner and outer diameters of the channel are 70 mm and 100 mm, respectively. The magnetic field is generated with a soft magnetic circuit and two series-connected circumferential coils. As will be shown shortly, the excited field topology is very similar to that of the SPT-100. The field intensity can be adjusted conveniently by varying the coil current.



Fig. 1. P100 Hall thruster.

Previous experimental experience tells that when a US Hall thruster with a brand-new straight channel discharges about two hours accumulatively, the walls become black and white. Hereby, a pre-discharge experiment on the P100 is performed over several hours to determine the wall section that needs to be chamfered. The operation conditions of the pre-discharge experiment are a discharge voltage U_{d} of 300 V and an anode mass flow rate $\dot{m}_{\mathrm{A}}$ of 5 mg/s. The propellant gas is xenon. In addition, the coil current is chosen such that the maximal anode efficiency is reached. On the basis of the above preparation, the chamfered channel wall is manufactured with the profile of the chamfered part linear for simplicity.

For experimental diagnosis, the thrust T and discharge current I_{d} are measured. T is obtained with a three-wire tor-

sion pendulum thrust stand. The measurement principle is to equalize the thrust to the rotation angle of the torsion platform, and then to convert the rotation angle into the linear displacement of a laser beam, so that the linear displacement is in direct proportion to the thrust. A standard weight is used online to calculate and calibrate the thrust. Its absolute accuracy is 0.4 mN.[17] The discharge current I_d is measured with a Tektronix TCP2020 current probe, and acquired and recorded using a Yokogawa DL850E ScopeCorder; the recorded time series data are then numerically processed to obtain the mean and peak-to-peak values of the discharge current. Besides, the anode efficiency η_a is calculated using Eq. (1). To facilitate a better understanding of the chamfered wall effect, the radial distribution of the ion current density at the axial position 10 cm away from the thruster exit is measured with a fast-sweeping Faraday probe.

$$\eta_a = \frac{T^2}{2\dot{m}_A U_d I_d}. \tag{1}$$

All the experiments are conducted in a vacuum tank at the Harbin Institute of Technology. The tank has a length of 5 m and an inner diameter of 2 m. The base pressure can reach 1.0×10^{-4} Pa. With the discharge of the P100 at a xenon mass flow rate of 5 mg/s, the working pressure corrected for xenon is about 3.0×10^{-3} Pa.

2.2. Numerical model and method

In order to reveal the underlying physics of the experimental findings for the chamfered wall effect, a numerical model which is solved using a particle-in-cell (PIC) technique is applied to simulate the discharge process inside the P100. Our group has previously established a PIC platform, which is capable of simulating the Hall thruster discharge.[18] The platform regards the propellant neutrals as a fluid flow and solves only its axial density distribution to accelerate the convergence. In this study, the platform is updated by treating the neutrals as individual particles, such as electrons and ions, to reflect a more realistic state of propellant dynamics. Therefore, it is a full PIC simulation.

Taking into account the axial symmetry of the Hall thruster structure, one can deem that the discharge is uniform along the azimuthal direction, and only the variations in the axial cross-section need to be considered. Therefore, the simulation model is built in the axial (z) and radial (r) planes, as shown in Fig. 2. The chamfer angles of the inner and outer walls are labeled as θ_i and θ_o, respectively. The line with $r = 0$ represents the thruster axis. The radial dimensions of the channel are identical to that of the P100. The envelope length and height of the domain are 60 mm and 100 mm, respectively.

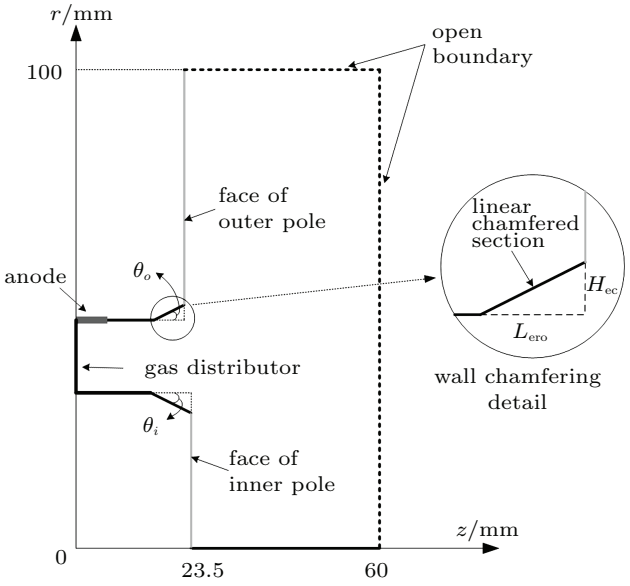


Fig. 2. Simulation domain for P100 discharge.

The neutrals are treated as a free molecular flow, while charged particles are driven under the combined effect of electric and magnetic fields and obey Newton's laws. The magnetic field is static and derived from the magnetic circuit model of the P100, which was preliminarily established and solved with a freeware package, namely finite element method magnetics (FEMM).[19] The electric field, which rises from the non-neutrality of local charge, is obtained by solving the Poisson equation. With respect to the collision between particles, only single ionization, excitation, and elastic collision between electrons and neutrals are considered. In addition, a Bohm-type collision is taken into account to compensate for the insufficient electron cross-field mobility. When a Bohm-type collision occurs, the electron is elastically scattered in the axial and azimuthal planes.[20] The collision frequency is described as $\nu_B = C_B eB/m_e$, where C_B is an empirical coefficient. It is well-known that based on the current knowledge of Hall thruster physics, no model can exactly describe the electron migration in a transverse magnetic field.[21] It has been suggested that the value of C_B outside the channel is greater than that inside the channel.[22] In this study, C_B is adjusted in each simulation case to match the measured discharge current.

The simulation domain inside the channel includes three solid boundaries. The left boundary represents the gas distributor; the propellant neutrals enter into the channel through this boundary with a half-Maxwellian distribution. The anode of P100, which is different from that of SPT100, is a metal ring attached on the outer wall near the channel bottom. Therefore, the upstream part of the upper boundary is the anode. By reaching either the gas distributor or the anode, the neutrals are diffusely reflected, the electrons are absorbed, and the ions are neutralized and re-enter into the channel. The discharge current is the sum of the anode electron and ion currents, and

is calculated as $I_{\rm d} = e(N^{\rm A}_{{\rm e},\Delta t} - N^{\rm A}_{{\rm i},\Delta t})/\Delta t$, where $N^{\rm A}_{{\rm e},\Delta t}$ and $N^{\rm A}_{{\rm i},\Delta t}$ are the respective numbers of electrons and ions reaching the anode per time step Δt. The potential on the anode is set as the discharge voltage exactly. The metallic gas distributor is floating and has a capacitance value of 1.0×10^{-8} F. Its potential is calculated as $\phi = Q/C$, where Q is the net charge accumulated by the distributor surface. The downstream part of the upper boundary as well as the entire lower boundary is the insulator wall, where secondary electron emission (SEE) due to electron bombardment is considered. The SEE model has been addressed elsewhere.[23–25] When heavy particles hit the insulator wall, the neutrals are also diffusely reflected, and the ions are recombined into neutrals and scattered. The wall potential is floating and the normal electric field is calculated as $E_{\rm n} = -\sigma/2\varepsilon_0$, where σ is the net surface charge density and ε_0 is the vacuum permittivity. Further treatment of the particle-boundary interaction, such as the energy accommodation, can be found elsewhere.[26]

The simulation domain outside the channel is semi-open. The left boundary, except the channel exit, is the faces of the inner and outer magnetic poles. Since these faces are metallically floating, they are treated using the same method as that used for the gas distributor. The lower boundary is the symmetry axis of the P100, so it is a mirror-reflecting boundary and the normal electric field there is zero. The upper and right boundaries are open; all species of particles are deleted from the program when they pass through. By integrating the flux and momentum of those deleted ions, the simulated ion current $I_{\rm i}$, thrust T, and propellant utilization $\eta_{\rm u}$ can be calculated as

$$\begin{aligned} I_{\rm i} &= eN^{\rm O}_{{\rm i},\Delta t}/\Delta t, \\ T &= m_{\rm i}\sum_{j=1}^{N^{\rm O}_{{\rm i},\Delta t}} u_{{\rm i}z,j}/\Delta t, \\ \eta_{\rm u} &= m_{\rm i} I_{\rm i}/e\dot{m}_{\rm A}, \end{aligned} \tag{2}$$

where $N^{\rm O}_{{\rm i},\Delta t}$ is the number of ions crossing the open boundaries, and $m_{\rm i}$ and $u_{iz,j}$ are the ion mass and axial velocity, respectively. The open boundaries are also quasi-neutral, which is guaranteed by supplying extra electrons into the boundary cells that are positively charged. The boundary potential is set zero.

The numerical methods adopted to solve the particle movement, electric potential, and particle collision are the leap-frog algorithm,[27] dynamic ADI algorithm,[28] and MCC algorithm based on null collision,[29] respectively. Rectangular meshes are used to discretize the simulation domain. Since the chamfered sections of both the inner and outer channel walls are sloped, they are approximated as a series of staircase steps to conform to the rectangular mesh. Moreover, as the use of real physical parameters in the full PIC simulation would result in a significant and unacceptable computation time cost, a technique proposed by Szabo for speeding up the simulation is applied to the model.[30] The technique decreases the mass of the heavy particles (neutral and ion) M by a factor of f and increases the vacuum permittivity ε_0 by a factor of γ^2, which could reduce the total simulation time by a factor of $\gamma\sqrt{f}$. In Szabo's latest work,[31] it was suggested that $f = 625$ and $\gamma = 20$ would generate a satisfactory result, which agrees well with experimental data. Accordingly, we choose the same f (625) but a smaller γ (12) here to obtain a more convincing result.

To justify the simulation, it is planned to compare the wall erosion based on the simulation results with the actual wall erosion observed in the pre-discharge experiment. The simulated wall erosion is quantified with the sputtering erosion rate ε, which is the result of the combined effect of the ion incident current density $j_{\rm i\perp}$, kinetic energy K, and angle θ on the wall, as expressed in Eq. (3)

$$\varepsilon = j_{\rm i\perp} f_\theta(\theta) f_K(K), \tag{3}$$

where f_θ and f_K are the sputtering yields due to the ion incident angle and energy, respectively. $j_{\rm i\perp}$, K, and θ can be obtained based on the statistics of the quantities of the individual ions which impact the wall, and f_θ and f_K are calculated based on the models proposed in Ref. [14].

A maximum of 7476 meshes (84×89) are used in the practical simulation depending on the magnitude of the wall chamfer angle. For each species of super-particle, a total number of $\sim 2.5 \times 10^5$ particles are simulated to guarantee an average number of ~30 in each mesh cell. Moreover, to save the computation time, the numbers, positions, and velocities of ions and neutrals are updated per 10 and 200 electron time steps, which is validated to have little influence on the result. The simulation takes typically 10 days of CPU time on a 3.6 GHz personal computer for convergence.

3. Results and analysis

3.1. Measurements in different wall chamfer angle cases

First of all, it is necessary to introduce the pre-discharge experiment results in the case of a brand-new straight channel. As shown in Fig. 3(a), with the increase of the coil current (namely the magnetic field intensity), the discharge current first drops down sharply, then decreases slowly in the coil current range of 3.3 A–4.8 A (from which the nominal operation condition of a Hall thruster is usually picked), and finally increases moderately. The variation range is large (up to 0.6 A). Besides, as shown in Fig. 3(b), the oscillation amplitude of the discharge current has a very similar variation to that of the discharge current and is at a consistent low-level in the

coil current range of 3.3 A–4.5 A. Nevertheless, the change of the thrust is completely reversed. One can see from Fig. 3(c) that, with the increase of the coil current, the thrust increases rapidly first and then decreases; the variation range is as great as 3 mN and the high thrust is achieved in the coil current range of 3.3 A–4 A. The above magnetic mapping characteristics accord well with those found in many other Hall thrusters with straight channels.[32–34] The distinct variations between the discharge current and the thrust lead to the variation of the anode efficiency as shown in Fig. 3(d). One can see that the coil current in the range of 3.5 A–4.3 A is favorable for the efficient operation, where the anode efficiency is above 48.5%. Besides, the anode efficiency is peaked at 49.3% when the coil current is 3.8 A.

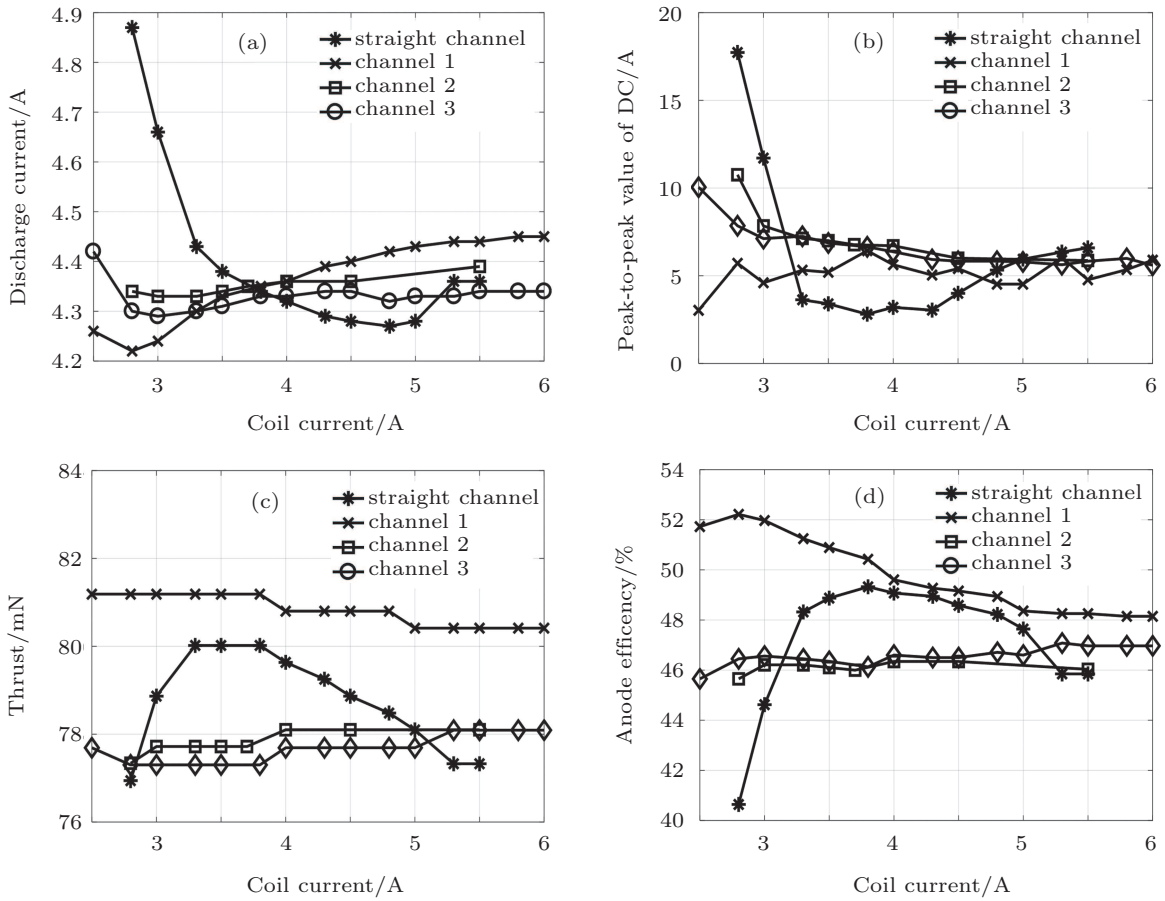


Fig. 3. Measured (a) discharge current, (b) peak-to-peak value of discharge current (DC), (c) thrust, and (d) anode efficiency versus coil current at different chamfered wall cases with $U_{\rm d} = 300$ V and $\dot{m}_{\rm A} = 5$ mg/s.

Under the condition that the peak anode efficiency is reached, the P100 with the brand-new straight channel endures a continuous discharge for about three hours. As shown in Fig. 4, the lengths of the erosion belts on the inner and outer walls $L_{\rm ero,i}$ and $L_{\rm ero,o}$ are measured to be 9 mm and 6 mm, respectively. Three chamfered wall configurations are hereby determined with their dimensions listed in Table 1, in which the chamfer angle θ is calculated as

$$\theta = \tan^{-1}\frac{H_{\rm ec}}{L_{\rm ero}}, \tag{4}$$

where $H_{\rm ec}$ is the thickness that is cut on the wall edge and $L_{\rm ero}$ is the length of the erosion belt, the schematic of which is shown in Fig. 2. Limited to the finite thicknesses of the straight channel walls, the chamfered wall case with a greater angle is not considered.

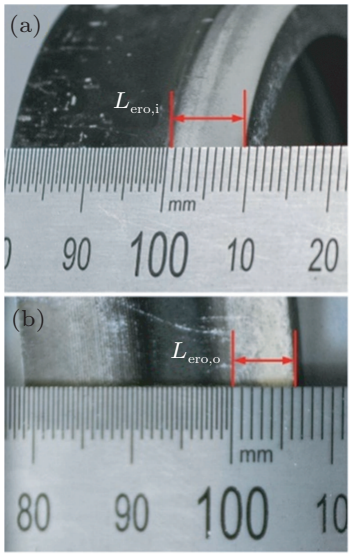


Fig. 4. (color online) Erosion belts of both (a) inner and (b) outer walls.

Table 1. Parameters of chamfered channel walls.

Channel	Inner wall		Outer wall	
	$H_{ec,i}$/mm	$\theta_i/^\circ$	$H_{ec,o}$/mm	$\theta_o/^\circ$
1	3	18.4	2	18.4
2	4.5	26.6	3.5	30.3
3	6	33.7	5	39.8

Using the same operating conditions as those in the pre-discharge experiment, the discharge characteristics of the P100 with different chamfered walls are measured. One can see obviously from Fig. 3 that the magnetic mapping characteristics in all the chamfered wall cases are much different from those in the straight channel case. In the case of channel 1, the discharge current increases gradually over most of the range of coil current and the variation range is small (less than 0.25 A); meanwhile, the oscillation amplitude is almost unchanged and the thrust decreases slowly with a total change less than 1 mN. The minimal discharge current is obtained at the coil current of 2.8 A, which is much lower than that (4.8 A) in the straight channel case. Furthermore, the parameter changes in both cases of channels 2 and 3 are fairly gentle and almost the same. When the coil current is beyond 2.8 A, the discharge current tends to increase, yet the increase rate is much smaller than that in the case of channel 1; besides, the oscillation amplitude decreases gradually while the thrust increases gradually with a total change about 0.5 mN.

The above results indicate that the discharge characteristics of a Hall thruster with the channel wall chamfered on the erosion belt are much less sensitive to the magnetic field intensity than those of a Hall thruster with a straight channel. Moreover, the greater the wall chamfer angle is, the weaker the effect of magnetic field intensity is. This finding is novel and unexpected. The only thing that can be certain is that this discrepancy is related to the change in the plasma-wall interaction due to the chamfering of the walls. However, the internal physics is hardly obtained due to the limitation of current knowledge. In principle, the electron cross-field mobility as well as the discharge current should be inversely proportional to the magnetic field intensity when the electrons are magnetized; nevertheless, the measured discharge current shows an increase with the field intensity at a certain range, and this range is greatly enlarged when the channel wall is chamfered (see Fig. 3(a)). Therefore, the magnetic mapping characteristics, especially when the channel wall is chamfered, are hard to be explained at present. In other words, the analysis on the variation of the discharge current with the wall chamfer angle in the whole coil current range is impractical, particularly when the variation trends below 3.5 A and beyond 4.3 A are quite different.

Anyhow, in respect of the quantitative change of the discharge performance in the coil current range of 3.5 A–4.3 A, where the P100 operates efficiently with the straight channel, both the thrust and the anode efficiency increase first and then decrease with the wall chamfer angle entirely, as shown in Figs. 3(c) and 3(d). The maximums are reached in the case of channel 1. That is to say, a modest chamfering of the channel wall is favorable to optimize the performance of Hall thrusters.

Figure 5 presents the measured ion current profiles at the coil current of 3.8 A, at which the peak anode efficiency in the case of the straight channel is reached. One can see that the maximum of the ion current density declines and the full width at half maximum (FWHM) of the distribution expands with the increase of the wall chamfer angle. The reason is that the chamfering of the wall leads to the augmentation of the channel cross-sectional area near the channel exit, which causes an extension of the radial space for ion inhabitancy and consequently a decrease of the radial span of high ion density. It is noted that all the measured profiles are non-centrosymmetric. This is because although the collection plate of the Faraday probe was calibrated to be parallel to the exit plane of the P100 before the experiments, the thrust generated from the discharge creates a deflection of the torsion balance as well as the thruster and consequently the probe does not sweep strictly along the thruster radial direction during the measurement.

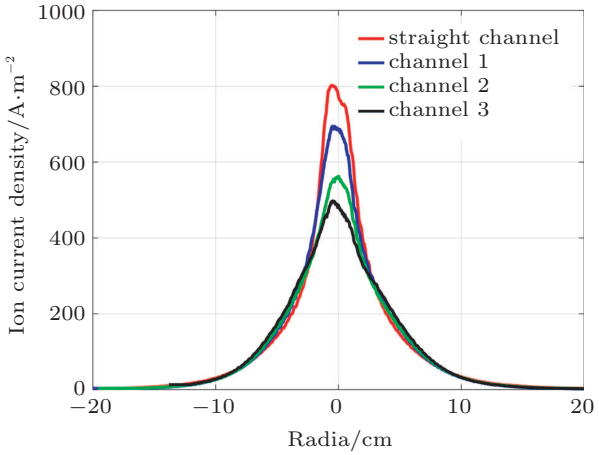


Fig. 5. (color online) Measured radial distribution of the ion current density at different chamfered wall cases with $U_d = 300$ V and $\dot{m}_A = 5$ mg/s.

3.2. Analysis of the driving mechanism based on simulation results

The most important finding in the experiments is that the high performance in the straight channel case can be further promoted by chamfering the channel wall moderately. It is thus necessary to probe into the corresponding discharge mechanisms with simulation. The simulation parameters then need to be determined. The discharge voltage, anode mass flow rate, and wall chamfer angles are selected as those used in the experiments. Besides, as both the discharge current and

thrust of the P100 with the straight channel change little (less than 3% and 1%, respectively, obtained from Figs. 3(a) and 3(c) in the coil current range of high performance (i.e., 3.5 A–4.3 A), only the magnetic field corresponding to the coil current of 4 A is chosen. We have explained above that it is not capable to analyze together the cases of the coil current below 3.5 A and beyond 4 A at present; therefore, they are not considered in the simulation. Furthermore, the employed empirical Bohm coefficients for each channel case are listed in Table 2, which are determined by cut-and-try method to reach the measured discharge current. It can be seen that only the coefficient inside the channel is adjusted while the coefficient outside the channel is unchanged. This treatment may be a rough approximation, but it is reasonable since the change of anomalous electron mobility, if any, originates exclusively from the change of the channel configuration. In the remainder of the paper, the chamfer angle of the inner wall is used to represent the different channel cases for the convenience of plotting the simulation result.

Table 2. Empirical Bohm coefficients used in the simulation.

Case	Inside channel	Outside channel
0°	1/140	1/16
18.4°	1/125	1/16
26.6°	1/105	1/16
33.7°	1/100	1/16

The magnetic field topology used in the simulation is presented in Fig. 6, accompanied by the converged steady distributions of plasma density for all the channel cases. It can be seen that the area of high plasma density is concentrated in the upstream half channel, which is closer to the anode than to the exit. Moreover, the density peak decreases monotonically with the increase of the wall chamfer angle, while its position is almost unchanged. With the subsequent ion acceleration, the erosion belts are formed on both the inner and outer walls downstream of the high-density area. As shown in Fig. 7, the simulated wall erosion rate in the straight channel case indicates that the lengths of the erosion belts $L_{\mathrm{ero,i}}$ and $L_{\mathrm{ero,o}}$ are 10 mm and 6.5 mm respectively, which are very close to those observed in the experiment. The simulation is thus justified to a certain extent.

The simulated discharge current obtained with the tabulated empirical coefficient is almost the same as the measured one, as shown in Fig. 8(a); the maximum relative difference is less than 1%. Moreover, as shown in Figs. 8(b) and 8(c), the simulated thrust and anode efficiency present the same variations as the measured ones; both of them increase first and then decrease with the wall chamfer angle. Although the discrepancy of the anode efficiency between the simulation and measurement is relatively large compared with those of the discharge current and thrust, it is still as small as 5%.

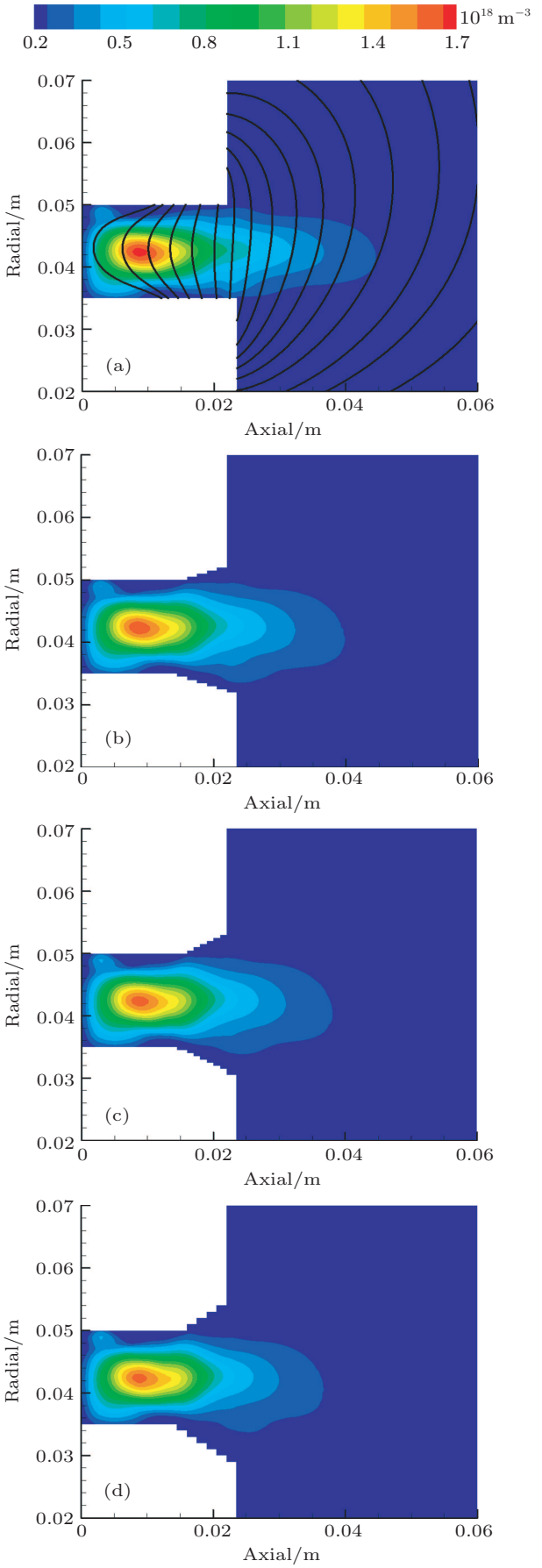


Fig. 6. (color online) Plasma density contours at wall chamfer angles of (a) 0°, (b) 18.4°, (c) 26.6°, and (d) 33.7°. Also presented is the magnetic field configuration used in the simulation. The discharge voltage is 300 V and the anode mass flow rate is 5 mg/s.

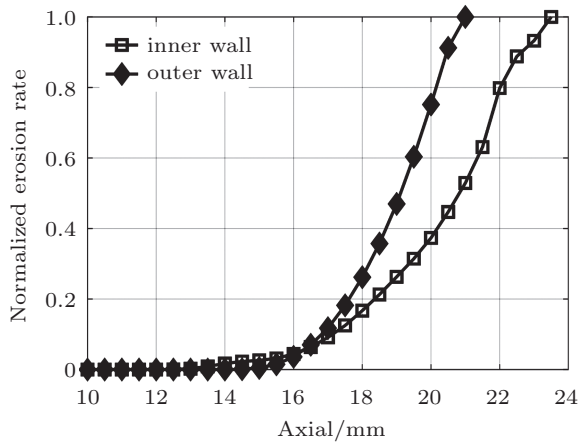


Fig. 7. Axial distribution of normalized erosion rate estimated with simulated ion parameters on the wall in the straight channel case.

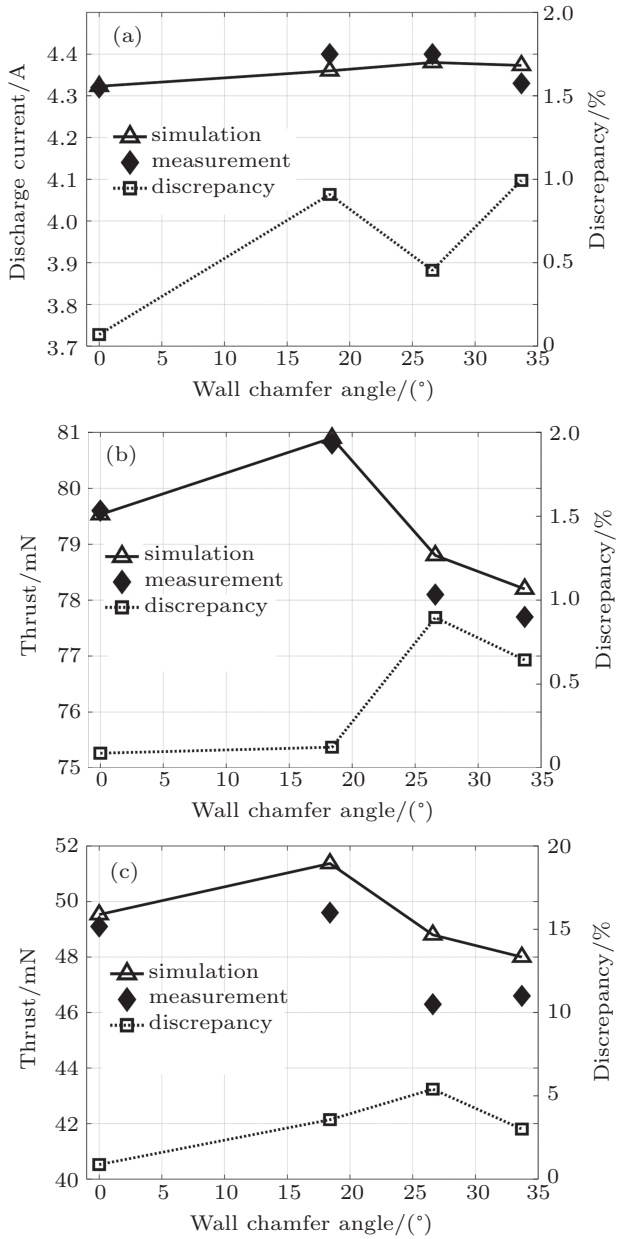


Fig. 8. (a) Discharge current, (b) thrust, and (c) anode efficiency versus wall chamfer angle and the discrepancy between the simulation and measurement results. The discharge voltage is 300 V and the anode mass flow rate is 5 mg/s.

It is noted that the optimal wall chamfer angle at which the thrust and anode efficiency reach their maximum values is approximately 20°, which is very close to the one determined in experiments. Therefore, both the measurement and simulation confirm that a Hall thruster designed with a straight channel configuration does not necessarily have an optimum performance. As such, a chamfered channel configuration deserves attention when designing a powerful Hall thruster.

As the discharge current changes little with the wall chamfer angle, the variation of the thruster performance is dominated by the variation of the thrust. Hence, the mechanism involved in the thrust variation is analyzed below. The thrust T is the reaction of ejection of those energetic ions out of the channel, and so can be calculated as

$$T = \dot{m}_{\mathrm{i}} V_{\mathrm{iz}}, \tag{5}$$

where $\dot{m}_{\mathrm{i}}$ is the ion mass flux, which can be obtained by counting the number of ions that escape the simulation domain from the downstream open boundaries per unit time. V_{iz} is the average axial velocity of those escaping ions, which is dominated by the acceleration electric field. Therefore, the interpretation of the thrust variation should originate from both the propellant utilization and the potential distribution.

There are two likely reasons for the absence of the maximum thrust in the straight channel case. Firstly, the ion acceleration efficiency with a straight channel is smaller than that with a chamfered channel. As shown in Figs. 9 and 10, as the wall chamfer angle increases, the potential inside the channel increases, the peak position of the ionization rate is unchanged, and the FWHM of the ionization rate curve is narrowed. Combining these two distributions, one can obtain that the plasma potential at the peak location of the ionization rate is the lowest in the straight channel case; therefore, the majority of ionized propellant receives the weakest acceleration when arriving the downstream open boundaries in this case. Secondly, the propellant utilization with a straight channel is not the biggest. It is well known that part of the ions would inevitably collide with the channel walls and be neutralized in the acceleration region, owing to the existence of the radial thermal pressure and electric field.[35] As the mean free path of ion-wall collision can be regarded as the channel width, it is the shortest in the straight channel case, and so the collision frequency as well as the neutralized ion population is the biggest. This is evidenced in Figs. 10 and 11. One can see that in the straight channel case, the ionization rate in the ionization region is the greatest; the neutral density therefore drops down to the lowest level there. However, in the vicinity of the channel exit, the ionization rate becomes the greatest again; the neutral density also becomes the biggest. The only reasonable explanation is the reentrance of those neutralized ions into the plasma bulk. Therefore, the effect of ion recombination on

the wall lowers the propellant utilization with a straight channel. Figure 12 presents the utilization efficiency by integrating the flux of the escaping ions. One can see that the propellant utilization is indeed depressed in the straight channel case. In summary, due to the combined effect of the weak acceleration and intense wall recombination of the ionized propellant, it is difficult to guarantee the maximum thrust in the straight channel case.

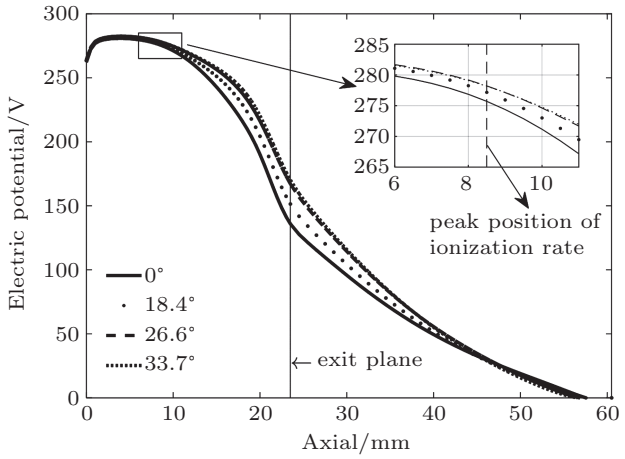


Fig. 9. Simulated distribution of plasma potential along the channel centerline at different channel cases.

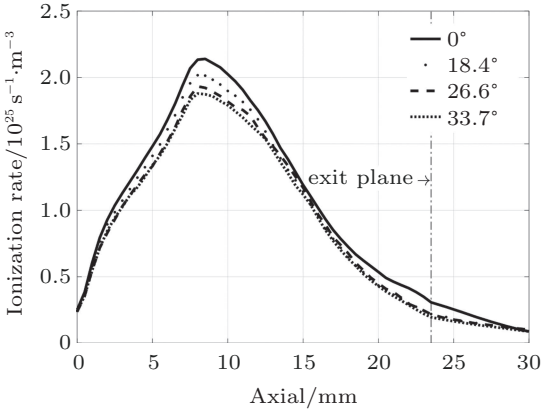


Fig. 10. Simulated distribution of ionization rate along the channel centerline at different channel cases.

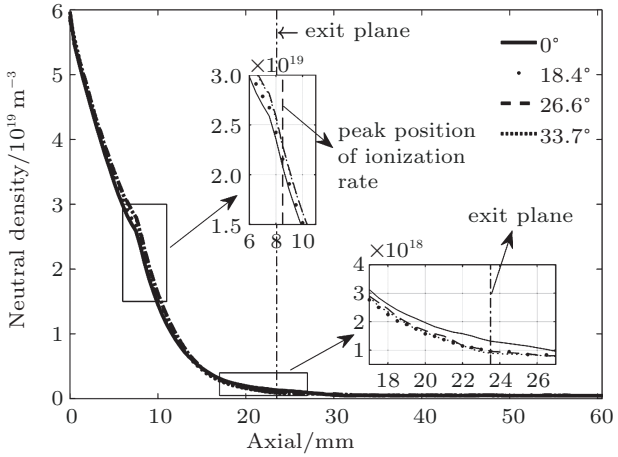


Fig. 11. Simulated distribution of neutral density along channel centerline near channel exit at different channel cases.

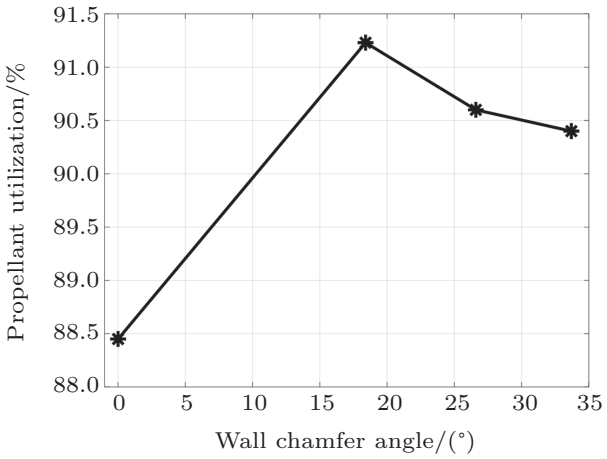


Fig. 12. Simulated propellant utilization versus wall chamfer angle.

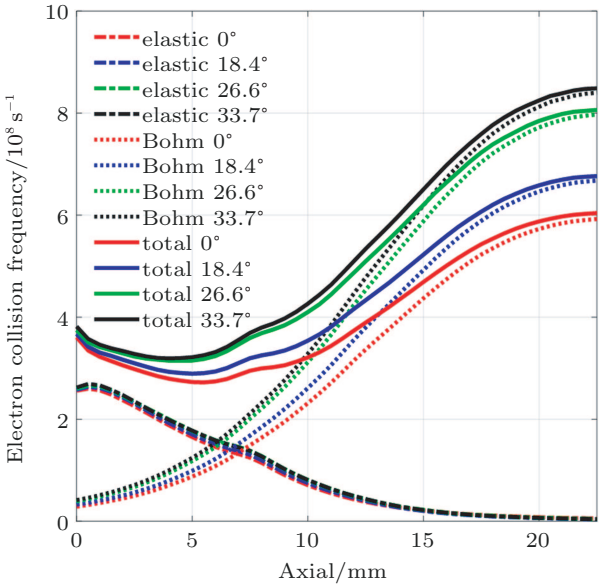


Fig. 13. (color online) Simulated distribution of electron collision frequency along channel centerline at different channel cases.

One point which deserves further discussion is the distribution of plasma potential shown in Fig. 9. It is well known that the potential distribution in a Hall thruster is the result of the distribution of electron cross-field mobility. When the magnetic field is fixed, the mobility is proportional to the electron collision frequency. The higher the frequency, the greater the mobility and the smaller the potential drop. From the simulated electron collision frequency shown in Fig. 13, one can see that most of the mobility is contributed by Bohm-type collision near the channel exit, whereas by electron-neutral elastic collision near the channel bottom. Neither the ionization frequency nor the excitation frequency is present since they are much smaller than the elastic frequency. In view that the plasma potential drops mainly in the downstream half section of the channel as shown in Fig. 9, the mobility due to the Bohm-type collision dominates the potential profile. As the

Bohm-type frequency increases gradually with the wall chamfer angle, the potential drop inside the channel decreases. Note that the variation of Bohm frequency is strongly correlated with the selection of the empirical Bohm coefficient listed in Table 2. Taking into account the good accordance between the measurement and the simulation, it is suggested that a chamfered wall promotes the anomalous mobility. However, the underlying physics is hard to be identified and beyond the scope of the present work. A specific study is necessary in the future to investigate this phenomenon.

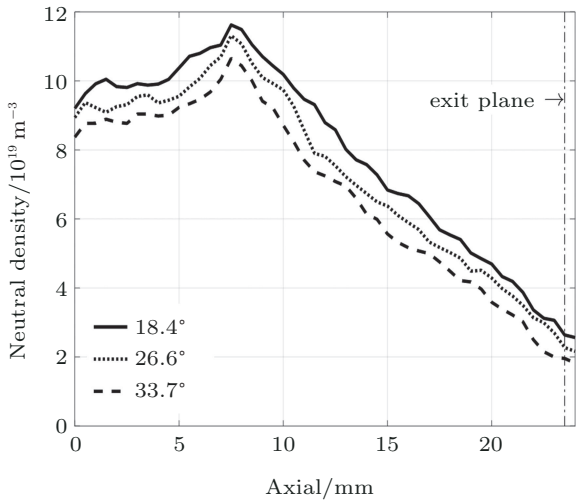


Fig. 14. Simulated distribution of neutral density along channel centerline before thruster ignition at different chamfered wall cases.

There are also two reasons which account for the decline of the thrust as the wall chamfer angle is increased excessively. Firstly, the propellant utilization decreases with the wall chamfer angle. The main cause is the change of the propellant flow distribution at an overlarge chamfer angle, which is different from the effect of ion recombination on the wall in the straight channel case. As shown in Fig. 14, with the increase of the wall chamfer angle, the propellant density inside the channel decreases monotonically before ignition, which inevitably leads to the global reduction of the ionization rate (see Fig. 10). This is a sign of propellant utilization loss. Secondly, the divergence loss of the ion beam increases with the wall chamfer angle. The channel chamfering results in a broadening of the channel width and consequently an increase of the potential drop between the plasma bulk and the wall (see Fig. 15); the ion radial velocity thus increases. However, figure 9 indicates that the ion acceleration voltage changes little at all the chamfered wall cases, which means that the final total velocities of the ions are almost the same. Therefore, the ion axial velocity decreases with the wall chamfer angle as shown in Fig. 16. The divergence loss of the ion beam thus increases. This argument can be verified by the measured ion current profiles in Fig. 5. As only the ion axial velocity contributes to the thrust, it is deduced that some thrust is lost when the wall chamfer angle is overlarge.

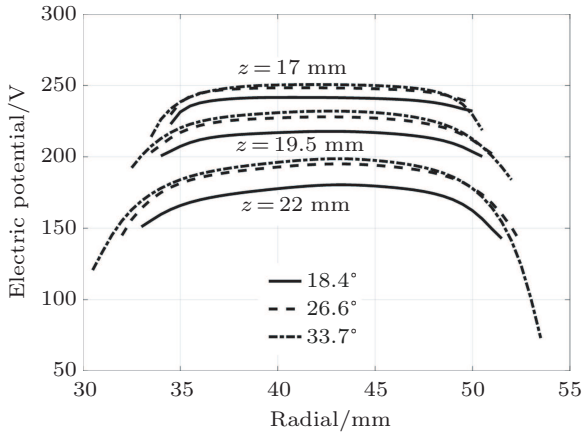


Fig. 15. Simulated radial distribution of plasma potential at different chamfered wall cases.

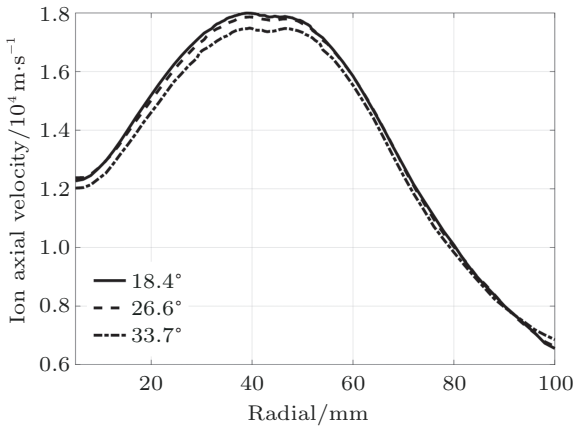


Fig. 16. Simulated radial distribution of the ion axial velocity on the downstream open boundary at different chamfered wall cases.

4. Conclusion and perspectives

The influence of a chamfered channel wall on the discharge of an unshielded Hall thruster has been investigated using a combination of experimental measurements and numerical simulations in this paper. The optimal performance of a Hall thruster is not necessarily achieved with a straight channel. A channel with a chamfered wall would be favorable to further improve the thruster performance. Specifically, a moderate chamfering can increase the ion acceleration voltage and reduce the ion recombination on the wall effectively; besides, it hardly disturbs the distribution of both the propellant flow and the plasma potential. These effects guarantee an improvement of propellant utilization and acceleration, and consequently an overall improvement of the performance.

A valuable and currently unexplained finding in this study is the significant variation of the magnetic mapping characteristics of Hall thrusters with the wall chamfering, which indicates a great change in the electron cross-field transport. At present, all existing investigations concerning the electron

transport focus on the situation of straight channel configuration, from which electron drift instability has been proposed to account for the anomalous mobility.[36–38] Therefore, in order to understand the effect of wall chamfering on the electron transport, the characteristics of electron drift instability as well as other discharge fluctuations, such as the rotating spike,[39] should be examined carefully in the case of chamfered channel configuration. The relevant work is on-going and will be reported soon. In addition, a further and similar study on a magnetically-shielded Hall thruster is also deserved and will be carried out in the future.

References

[1] Kozubskii K N, Murashko V M, Rylov Y P, Trifonov Y V, Khodnenko V P, Kim V, Popov G A and Obukhov V A 2003 *Plasma Phys. Rep.* **29** 251

[2] Mazouffre S 2016 *Plasma Sources Sci. Technol.* **25** 033002

[3] Sankovic J M, Hamley J A and Haag T W 1993 *23rd International Electric Propulsion Conference*, September 13–16, 1993, Seattle, USA, p. IEPC-1993-094

[4] Gopantchuk V, Kozubsky K, Maslennikov N and Pridannikov S 1999 *26th International Electric Propulsion Conference*, October 17–21, 1999, Kitakyushu, Japan, p. IEPC-1999-086

[5] Peterson P, Manzella D and Jacobson D 2003 *39th AIAA/ASME/SAE/ASEE Joint Propulsion Conference and Exhibit*, July 20–23, 2003, Huntsville, USA, p. AIAA-2003-5005

[6] Richard H, Dan G, Ioannis M and Ira K 2012 *48th AIAA/ASME/SAE/ASEE Joint Propulsion Conference & Exhibit*, July 30–August 1, 2012, Atlanta, USA, p. AIAA-2012-3788

[7] Conversano R W, Goebel D M, Hofer R R, Mikellides I G and Wirz R E 2017 *J. Propul. Power* **33** 975

[8] Mazouffre S, Vaudolon J, Largeau G, Hénaux C, Rossi A and Harribey D 2014 *IEEE Trans. Plasma Sci.* **42** 2668

[9] Mikellides I G, Katz I, Hofer R R, Goebel D M, de Grys K and Mathers A 2011 *Phys. Plasmas* **18** 033501

[10] Mikellides I G, Katz I, Hofer R R and Goebel D M 2013 *Appl. Phys. Lett.* **102** 023509

[11] Arhipov B, Goghaya E and Nikulin N 1998 *34th AIAA/ASME/SAE/ASEE Joint Propulsion Conference and Exhibit*, July 13–15, 1998, Cleveland, USA, p. AIAA-1998-3800

[12] Yamamoto N, Komurasaki K and Arakawa Y 2005 *J. Propul. Power* **21** 870

[13] Raitses Y, Ashkenazy J and Guelman M 1998 *J. Propul. Power* **14** 247

[14] Mikellides I G, Katz I, Hofer R R and Goebel D M 2014 *J. Appl. Phys.* **115** 043303

[15] Hofer R R, Goebel D M, Mikellides I G and Katz I 2014 *J. Appl. Phys.* **115** 043304

[16] Soulas G C 2013 *33rd International Electric Propulsion Conference*, October 6–10, 2013, Washington, USA p. IEPC-2013-157

[17] Li H, Ning Z and Yu D 2013 *J. Appl. Phys.* **113** 083303

[18] Liu H, Wu B Y, Yu D R, Cao Y and Duan P 2010 *J. Phys. D: Appl. Phys.* **43** 165202

[19] Meeker D 2013 femm Ver. 4.2 (http://www.femm.info)

[20] Smirnov A, Raitses Y and Fisch N J 2004 *Phys. Plasmas* **11** 4922

[21] Ahedo E 2011 *Plasma Phys. Controlled Fusion* **53** 124037

[22] Boniface C, Garrigues L, Hagelaar G J M, Boeuf J P, Gawron D and Mazouffre S 2006 *Appl. Phys. Lett.* **89** 161503

[23] Zhang F K and Ding Y J 2011 *Acta Phys. Sin.* **60** 065203 (in Chinese)

[24] Zhang F K, Ding Y J, Qing S W and Wu X D 2011 *Chin. Phys. B* **20** 125201

[25] Duan P, Qin H J, Zhou X W, Cao A N, Chen L and Gao H 2014 *Chin. Phys. B* **23** 075203

[26] Szabo J, Warner N, Martinez-Sanchez M and Batishchev O 2014 *J. Propul. Power* **30** 197

[27] Birdsall C K and Langdon A B 1991 *Plasma physics via computer simulation* (New York: Adam Hilger) p. 13

[28] Doss S and Miller K 1979 *SIAM J. Numer. Anal.* **16** 837

[29] Vahedi V and Surendra M 1995 *Comput. Phys. Commun.* **87** 179

[30] Szabo J 2001 "Fully Kinetic Numerical Modeling of a Plasma Thruster", Ph. D. Dissertation (Massachusetts: Massachusetts Institute of Technology)

[31] Szabo J, Warner N, Martinez-Sanchez M and Batishchev O 2014 *J. Propul. Power* **30** 197

[32] Sekerak M J, Gallimore A D, Brown D L, Hofer R R and Polk J E 2016 *J. Propul. Power* **32** 903

[33] Gascon N, Dudeck M and Barral S 2003 *Phys. Plasmas* **10** 4123

[34] Wei L, Wang C, Han K and Yu D 2012 *Phys. Plasmas* **19** 012107

[35] Keidar M, Boyd I D and Beilis I I 2001 *Phys. Plasmas* **8** 5315

[36] Croes V, Lafleur T, Bonaventura Z, Bourdon A and Chabert P 2017 *Plasma Sources Sci. Technol.* **26** 034001

[37] Héron A and Adam J C 2013 *Phys. Plasmas* **20** 082313

[38] Cavalier J, Lemoine N, Bonhomme G, Tsikata S, Honoré C and Grésillon D 2013 *Phys. Plasmas* **20** 082107

[39] Sekerak M J, Gallimore A D, Brown D L, Hofer R R and Polk J E 2016 *J. Propul. Power* **32** 903